Eur Biophys J (2015) 44:235–247
DOI 10.1007/s00249-015-1018-9

ORIGINAL PAPER

EBSA
Biophysics in Europe

Characterization of the flexible lip regions in bacteriophage lambda lysozyme using MD simulations

Lorna J. Smith[1] · **Wilfred F. van Gunsteren**[2] · **Niels Hansen**[2,3]

Received: 13 January 2015 / Revised: 27 February 2015 / Accepted: 5 March 2015 / Published online: 28 March 2015

Abstract The upper and lower lip regions in lysozyme from bacteriophage lambda (λ-lysozyme) are flexible in solution and exhibit two different conformations in crystal structures of the protein. MD simulations have been used to characterize the structure and dynamics of these lip regions, which surround the active site. Ten different simulations have been run including those with restraining to experimental NOE distance and ^{1}H-^{15}N order parameter data. The simulations show that the lower lip region, although undergoing considerable backbone fluctuations, contains two persistent β-strands. In the upper lip region, a wide range of conformations are populated and it is not clear from the available data whether some helical secondary structure is present. The work provides a clear example of the advantages of combining MD simulations with experimental data to obtain a structural interpretation of the latter. In this case, time-averaged order parameter restraining has played an essential role in enabling convergence between two different starting structures and identifying the extent to which flexible regions in solution can contain persistent secondary structure.

Keywords Lysozyme · Order parameter · ^{15}N relaxation · Molecular dynamics simulation · GROMOS

Abbreviations

λ-lysozyme	Lysozyme from bacteriophage lambda
MD	Molecular dynamics
NMR	Nuclear magnetic resonance
NOE	Nuclear Overhauser Effect
PDB	Protein data bank
RMSD	Root-mean-square difference
RMSF	Root-mean-square fluctuation
SPC	Simple point charge

Introduction

Protein structures are inherently dynamic and can exhibit a wide variety of motional processes. These range from the fluctuations of side chains and loop regions, through the relative motions of domains and subunits, to, in extreme cases, large-scale rearrangements of the entire protein fold (Bahar et al. 2010; Henzler-Wildman and Kern 2007; Tokuriki and Tawfik 2009). Such intrinsic motions are increasingly recognized to be of fundamental importance to the functions of proteins. They have been shown to play a central role, for example, in molecular recognition, protein regulation, allosteric interactions, enzyme catalysis, and cellular signaling (Boehr et al. 2009; Fuxreiter 2012; Henzler-Wildman et al. 2007; Motlagh et al. 2014; Smock and Gierasch 2009). The internal motions enable an ensemble of conformations to be accessed, different conformers within the ensemble potentially contributing to the

Electronic supplementary material The online version of this article (doi:10.1007/s00249-015-1018-9) contains supplementary material, which is available to authorized users.

✉ Lorna J. Smith
lorna.smith@chem.ox.ac.uk

[1] Department of Chemistry, Inorganic Chemistry Laboratory, University of Oxford, South Parks Road, Oxford OX1 3QR, UK

[2] Laboratory of Physical Chemistry, Swiss Federal Institute of Technology ETH, Vladimir-Prelog-Weg 2, 8093 Zurich, Switzerland

[3] Institute of Thermodynamics and Thermal Process Engineering, University of Stuttgart, Pfaffenwaldring 9, 70569 Stuttgart, Germany

biological function in different ways (Frauenfelder et al. 1991; Lewney and Smith 2012; Sekhar and Kay 2013).

Lysozyme from bacteriophage lambda (λ-lysozyme) is an example of an enzyme in which significant conformational dynamics appear to play an important functional role (Evrard et al. 1999). λ-lysozyme is a lytic transglycosylase, catalyzing the cleavage of glycosidic bonds in bacterial peptidoglycan (Bienkowskaszewczyk et al. 1981; Black and Hogness 1969; Taylor et al. 1975). The 158-residue protein has a two domain structure that contains six α-helices (residues 6–19, 71–81, 88–101, 104–110, 113–121, 135–149) and six β-strands forming two β-sheets (residues 34–37, 40–42, 52–58, 59–61, 63–66, 68–70) (Fig. 1) (Evrard et al. 1998; Leung et al. 2001). The enzyme active site and essential catalytic residue, Glu 19, lie in a cleft between the two domains (Jespers et al. 1992). The lower and upper lip regions of the protein, residues 51–60 and 128–141, respectively, surround the active site. These lip regions have been shown, by ^{15}N NMR relaxation studies, to be undergoing motions on a picosecond timescale in solution, exhibiting reduced ^{1}H-^{15}N order parameters (Smith et al. 2013). Exchange contributions to T_2 are also observed for certain residues in the lip regions, reflecting slower timescale motions (Smith et al. 2013).

Interestingly, these lower and upper lip regions, which are dynamic in solution, show two different conformations in X-ray structures of λ-lysozyme (Evrard et al. 1998; Leung et al. 2001). In the X-ray structure where no inhibitor is bound in the active site [PDB code 1AM7 (Evrard et al. 1998)], there are three molecules, called A–C, in the asymmetric unit. Molecules A and C show an open conformation. In this form, the lower lip region contains two β-strands (β3 and β4) and the end of the upper lip region forms the first helical turn of helix α6 (residues 135–149). In contrast, molecule B in the 1AM7 X-ray structure displays a closed conformation. This closed form is also seen in the X-ray structure of a complex of λ-lysozyme with hexa-*N*-acetylchitohexanose [PDB code 3D3D (Leung et al. 2001)]. In the closed form, the β-strands in the lower lip are absent. This region instead forms a loop that partially restricts access to the enzyme active site. Similarly in the upper lip, the first turn of helix α6 is absent and the upper lip forms a loop that extends across the active site cleft (Fig. 1) (Evrard et al. 1998; Leung et al. 2001).

Analysis of the crystal structures, mutagenesis studies, and histidine modification experiments have provided evidence that both the open and closed forms of λ-lysozyme, and interconversion between them, are required for the enzyme function (Evrard et al. 1999). The open form is needed to allow entry of the peptidoglycan substrate to the active site, as in the closed form the opening is too small. However, the closed form appears to be necessary for enzyme activity. In particular, *N*-carbethoxylation of His 137 in the upper lip region, which would sterically prevent formation of the closed form, inactivates the enzyme. Mutation of His 137 to asparagine, though, which should retain the ability to form both the open and closed forms, has little or no effect on the enzyme activity (Evrard et al. 1999).

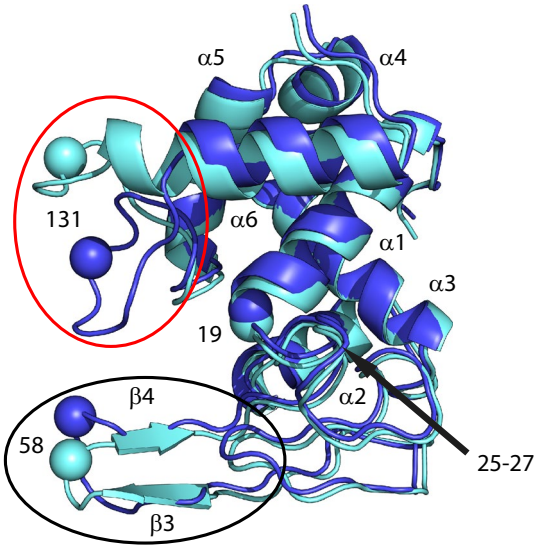

Fig. 1 The open (*cyan*) and closed (*blue*) conformations of lambda lysozyme seen in the 1AM7 X-ray structure (molecules A and B, respectively) (Evrard et al. 1998). The lower lip (residues 51–60) and upper lip (residues 128–141) regions are indicated by *black* and *red ovals*, respectively, and the six α-helices, β-strand β3 and β4 and the exposed loop residues 25–27 are labeled. The Cα atoms of residues 19, 58, and 131 are shown as colored spheres; the distances between these atoms are monitored through the simulations to assess changes to the lip regions (Figs. 4, 5, 6). The figure was produced using the PyMOL program (The PyMOL Molecular Graphics System, Version 1.6.0.0 Schrödinger, LLC)

In (Smith et al. 2013), two 10-ns simulations using the GROMOS 45A3 force field are reported and a number of properties are compared between simulation and experiment. In the present work, we characterize the dynamical properties of the lower and upper lip regions of λ-lysozyme using molecular simulation. Ten different 25-ns MD simulations using the GROMOS 54A7 force field have been run, five starting from the open conformation and five from the closed conformation present in the 1AM7 X-ray structures (Evrard et al. 1998). Two of the simulations are unrestrained, i.e., do not use the NMR data, while in the others restraints to experimental data have been applied as is done in protein structure refinement based on experimental X-ray or NMR data. The structure refinement MD simulations with restraining to a limited set of NOE distance and ^{1}H-^{15}N order parameter restraints show good structural equilibration and convergence. The simulation analysis is focused on the lower and upper lip regions. These populate a wide range of conformations during the simulations,

Table 1 Summary of the simulations of λ-lysozyme

Simulation name	Starting conformation	NOE restraints applied	Order parameter restraints applied
MD_O	1AM7: A open	No	No
MD_C	1AM7: B closed	No	No
NOE_O	1AM7: A open	Yes	No
NOE_C	1AM7: B closed	Yes	No
S2_ALL_O	1AM7: A open	No	Yes for all residues
S2_ALL_C	1AM7: B closed	No	Yes for all residues
S2_7_O	1AM7: A open	No	Yes for 7 residues
S2_7_C	1AM7: B closed	No	Yes for 7 residues
S2_NOE_O	1AM7: A open	Yes	Yes for 7 residues
S2_NOE_C	1AM7: B closed	Yes	Yes for 7 residues

The simulation name used, the starting structure for the simulation, and whether or not NOE and ^{1}H-^{15}N order parameter restraints were applied in the simulation are indicated. Further details are given in the Methods section and the NOE and order parameter restraints used are listed in the Supplementary Material

the trajectories showing good agreement with the available experimental data.

Materials and methods

The MD simulations were carried out using the GROMOS biomolecular simulation software (Eichenberger et al. 2011; Schmid et al. 2011a, 2012) (http://www.gromos.net) and the GROMOS 54A7 force-field parameter set (Schmid et al. 2011b). The simulations reported in this work are summarized in Table 1. The starting coordinates for the simulations were taken from the structures of λ-lysozyme with Protein Data Bank code 1AM7 (Evrard et al. 1998), using molecules A and B from the asymmetric unit for the open and closed conformation, respectively. The X-ray structure determination (at pH 6.7) had used a mutant form of λ-lysozyme in which all the tryptophan residues were converted into aza-tryptophan (Evrard et al. 1998). This enabled crystals suitable for X-ray analysis to be grown (Evrard et al. 1997). In addition, the last four residues are missing in the X-ray structure due to insufficient electron density. For the simulations, the wild-type sequence of λ-lysozyme was used with all the aza-tryptophan residues changed to tryptophan and the final four residues added to the structure in an extended conformation. In order to reproduce the pH conditions of the experimental NMR work (pH 5.45) (Di Paolo et al. 2010; Smith et al. 2013), in the simulations the Asp and Glu side chains in the protein were unprotonated and Cys 120 was protonated. In addition, His 31 and His 137 on the protein surface were doubly protonated and His 48, which is known experimentally to be uncharged at pH 5.45 (Soumillion and Fastrez 1998), was singly protonated at Nε2. For both the open and closed conformations, the protein was solvated in a rectangular box and minimum image periodic boundary conditions were applied. The minimum solute-box wall distance was set to 1.605 nm for the open conformation and 1.4 nm for the closed conformation giving, in both cases, 16,592 simple point charge (SPC) water molecules (Berendsen et al. 1981). Six chloride ions were added to achieve overall neutrality of the system.

For each simulation, an initial equilibration scheme comprising five 20-ps simulations at temperatures of 60, 120, 180, 240, and 300 K was used. During the first 80 ps of this equilibration, the solute atoms were harmonically restrained to their positions in the starting structure with force constants of 25,000, 2500, 250, and 25 kJ mol^{-1} nm^{-2} at temperatures of 60, 120, 180, and 240 K, respectively. Following equilibration the simulations were run at 300 K. All simulations were performed at a constant pressure of 1 atm, the temperature and pressure being maintained using the weak coupling algorithm (Berendsen et al. 1984), with relaxation times of $\tau_T = 0.1$ ps and $\tau_p = 0.5$ ps and an isothermal compressibility of 4.575×10^{-4} (kJ mol^{-1} nm^{-3})$^{-1}$. Protein and solvent were separately coupled to the heat bath. The SHAKE algorithm (Ryckaert et al. 1977) was used to constrain bond lengths and the geometry of the water molecules, with a relative geometric tolerance of 10^{-4} allowing for an integration time step of 2 fs. The center of mass motion was removed every 1000 time steps. Non-bonded interactions were calculated using a triple-range cutoff scheme with cutoff radii of 0.8 and 1.4 nm. Interactions within 0.8 nm were evaluated every time step and intermediate range interactions were updated every fifth time step. To account for the influence of the dielectric medium outside the cutoff sphere, a reaction-field force (Tironi et al. 1995) with a relative dielectric permittivity ε of 61 was used (Heinz et al. 2001).

Following equilibration, the simulations starting from the open and closed conformations were each branched into five different runs, which are summarized in Table 1.

In the NOE_O, NOE_C, S2_NOE_O, and S2_NOE_C simulations 22 time averaged (r^{-3}) NOE restraints were applied (Schmid et al. 2011a) with a force constant of 6,000 kJ mol^{-1} nm^{-2} and a memory relaxation time of 20 ps. The NOE distance restraints used are listed in Table S1 in the Supplementary Material. Only NOE atom pairs involving atoms of the lip regions were used because these are of primary interest when characterizing the lip motions. Likewise, in the S2_7_O, S2_7_C, S2_NOE_O, and S2_NOE_C simulations seven ^{1}H-^{15}N order parameter restraints involving residues in the lip regions were applied while in the S2_ALL_O and S2_ALL_C simulations ^{1}H-^{15}N order parameter restraints were applied (Hansen et al. 2014) for all residues where experimental data are available (128 residues). The order parameter restraints used are listed in Tables S2 and S3 in the Supplementary Material. A force constant of 100 kJ mol^{-1}, a memory relaxation time of 20 ps, and a flat bottom of $\Delta S^2 = 0.05$ were used. Simulations using larger force constants of 200, 300, and 400 kJ mol^{-1} and longer memory relaxation times of 50 and 100 ps were also investigated (data given in the Supplementary Material). However, the smallest force constant value of 100 kJ mol^{-1}, with a memory relaxation time of 20 ps, was found to be sufficient for satisfying the experimental data.

Analysis was performed with the GROMOS++ suite of analysis programs (Eichenberger et al. 2011) using coordinate and energy trajectories written to disk every 5 ps. Regions of secondary structure were identified using the rules defined by Kabsch and Sander in the program DSSP (Kabsch and Sander 1983). Hydrogen bonds were identified according to a geometric criterion: a hydrogen bond was assumed to exist if the hydrogen-acceptor distance is smaller than 0.25 nm and the donor-hydrogen-acceptor angle is larger than 135°. In the calculations of the backbone atom positional root-mean-square-differences (RMSD) of the protein structure in the simulations the four terminal residues, which were missing in the 1AM7 structure, were excluded. Inter-proton distances, derived from the NOE cross-peak intensities (Table S1), for residues in the lower and upper lip regions of the protein, were compared with the average inter-proton distances $\langle r^{-3} \rangle^{-1/3}$ calculated from the simulated trajectories. Because the GROMOS force fields make use of united atoms, positions of aliphatic hydrogen atoms were constructed based on standard geometries (van Gunsteren et al. 1996). Analysis of crystal contacts and intermolecular hydrogen bonds in the 1AM7 crystal structure was performed using the Protein interfaces, surfaces and assemblies service PISA at the European Bioinformatics Institute. (http://www.ebi.ac.uk/pdbe/prot_int/pistart.html) (Krissinel and Henrick 2007).

Results

The analysis reported in this paper concentrates on the behavior of the lower and upper lip regions (residues 51–60 and 128–141, respectively). A number of quantities are used to define their conformation.

The first quantity is the agreement of interproton distances calculated from the protein structure in the simulation trajectories with NOE interproton distance bounds. Although a detailed analysis of NOE data for λ-lysozyme has not been performed, NOE data for residues in the lip regions have been identified (Smith et al. 2013). From these data, a set of 22 NOE distance bounds is considered (Table S1, Supplementary Material) which define the β-sheet secondary structure in the lower lip (12 bounds) and the α-helical secondary structure at the start of helix α6 towards the end of the upper lip region (ten bounds). In the X-ray structures, all the upper lip NOE distance bounds are satisfied in both the open and closed conformations. However, in the lower lip, the open conformation shows one NOE bound violation greater than 0.05 nm and the closed conformation shows six bound violations greater than 0.05 nm, three of which are greater than 0.15 nm (Fig. 2 upper panels). So the crystal structures, in particular the closed form, derived from X-ray diffraction data are not wholly compatible with the NMR NOE data obtained for the protein in aqueous solution.

The second quantity is the persistence of five hydrogen bonds formed in the secondary structure regions in the lower and upper lips. These hydrogen bonds are 53NH-61CO, 61NH-53CO in the lower lip β-sheet and 138NH-134CO, 139NH-135CO and 140NH-136CO at the start of helix α6 in the upper lip. In the X-ray structures, in the open conformation the two hydrogen bonds in the lower lip region and the 140NH-136CO hydrogen bond are present but the other two helical hydrogen bonds are replaced by one i,i-3 hydrogen bond, 138NH-135CO. All five hydrogen bonds are missing in the closed conformation.

The third quantity is the distance between the Cα atoms of Lys 58 in the lower lip and Gly 131 in the upper lip and the distance of each of these atoms to the Cα atom of Glu 19 in the active site cleft (Fig. 1). The 58 Cα-131 Cα distance is significantly longer in the X-ray structure in the open conformation (2.43 nm) than in the closed conformation (1.35 nm). The same is seen for the distance 19 Cα-131 Cα (2.02 nm open and 1.43 nm closed), while the distance 19 Cα-58 Cα is similar in both conformations (1.96 nm open and 1.90 nm closed).

Initially, two 25-ns simulations of λ-lysozyme were run, one starting from the open conformation and the other from the closed conformation in the 1AM7 X-ray structure of λ-lysozyme (Evrard et al. 1998) (simulations MD_O and

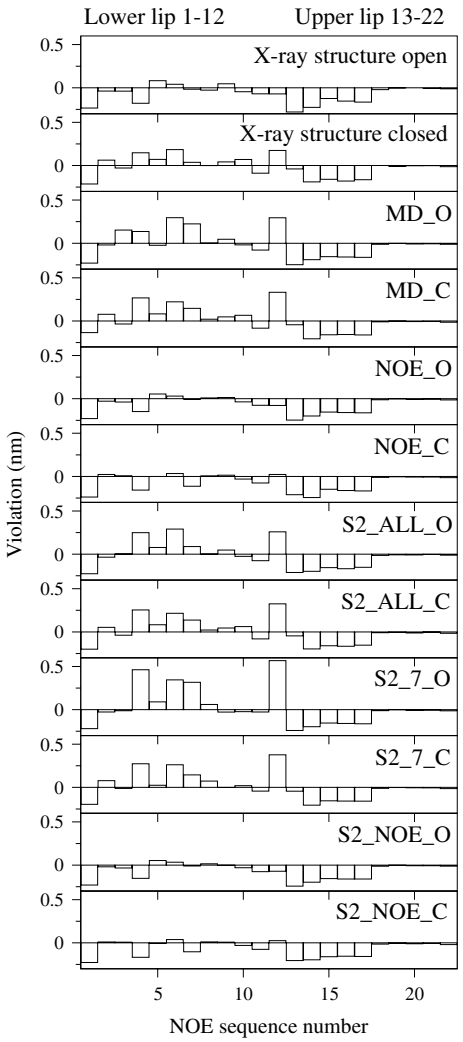

Fig. 2 Comparison of the $\langle r^{-3} \rangle$ averaged interproton distances in the simulations (over the time period 10–25 ns) with the upper distance bound derived from experimental NOE intensities (violation = simulated distance–distance upper bound; a negative violation shows that the distance bound is satisfied). NOE numbers 1–12 and 13–22 are for residues in the lower and upper lip regions, respectively. A list of the NOE distance bounds used in the restraints is given in Table S1 in the Supplementary Material

MD_C, respectively; Table 1). The backbone atom positional root-mean-square differences (RMSD) of the protein structure in the simulation compared to the starting crystal conformation (data given in the Supplementary Material) and the root-mean-square fluctuations (RMSF) of the backbone N atoms in the two simulations (see Fig. 7a, b discussed in detail later) have been analyzed. The largest fluctuations (>0.15 nm) are concentrated in the N and C-termini, an exposed loop between helix α1 and β-strand β1 (residues 25–27), and in the upper and lower lip regions. When these residues are excluded, the RMSD values level off to approximately 0.15 and 0.18 nm for the MD_O and MD_C simulations, respectively.

Simulations MD_O and MD_C satisfy all the experimental NOE interproton distance bounds (no. 13–22) for the upper lip region. However, for the lower lip region data (no. 1–12), these simulations show five and four NOE bound violations greater than 0.1 nm, respectively (Fig. 2, 3rd, 4th panels). All five secondary structure hydrogen bonds in the lip region are seen in the first section of the MD_O simulation but, after about 8 ns, the 61NH-53CO and 140NH-136CO hydrogen bonds are lost. None of the five hydrogen bonds are seen with a population greater than 0.1 % in the MD_C simulation (Fig. 3). For the distances involving the lower and upper lips (upper panels in Figs. 4, 5, 6), the distances 58 Cα-131 Cα (Fig. 6) and 19 Cα-131 Cα (Fig. 5) remain close to their values in the starting structures used for the simulations. Thus the mean 58 Cα-131 Cα distance is 2.67 and 1.16 nm in simulations MD_O and MD_C, respectively, and the mean for distance 19 Cα-131 Cα is 1.92 and 1.39 nm in the simulations MD_O and MD_C, respectively. In contrast, while the 19 Cα-58 Cα distance (Fig. 4) remains close to that seen in the starting structure in the MD_O simulation (dotted line, mean 1.82 nm), this distance becomes significantly shorter in the MD_C simulation (solid line, mean 1.36 nm).

The conformations in the lower and upper lip regions explored in the MD_O and MD_C simulations are clearly different. If there were adequate conformational sampling, we would expect the trajectories run from different starting structures to show the same conformational properties after equilibration. However, the secondary structure hydrogen bonds populations in the lip regions (Fig. 3) and the distances analyzed that involve these regions (Figs. 4, 5, 6) are significantly different in the two simulations. Both simulations show violations of the experimental NOE distance bounds in the lower lip region (Fig. 2) and the absence of the β-sheet secondary structure when starting from the closed conformation and a loss of one β-sheet hydrogen bond when starting from the open conformation (Fig. 3, hydrogen bonds 1 and 2). To address this, it was decided to apply a structure refinement protocol involving two 25-ns simulations, starting from the open and closed conformations in the X-ray structure and applying the 22 experimental NOE distance bound restraints for the lower and upper lip regions, with time averaging (simulations NOE_O and NOE_C, respectively; Table 1).

As expected, in both the NOE_O and NOE_C simulations, the experimental interproton distance bounds, which were used in the structure refinement protocol, are essentially satisfied (Fig. 2, 5th, 6th panels). The NOE_O and NOE_C simulations show no NOE violation greater than 0.06 and 0.04 nm, respectively. In the NOE_O simulation,

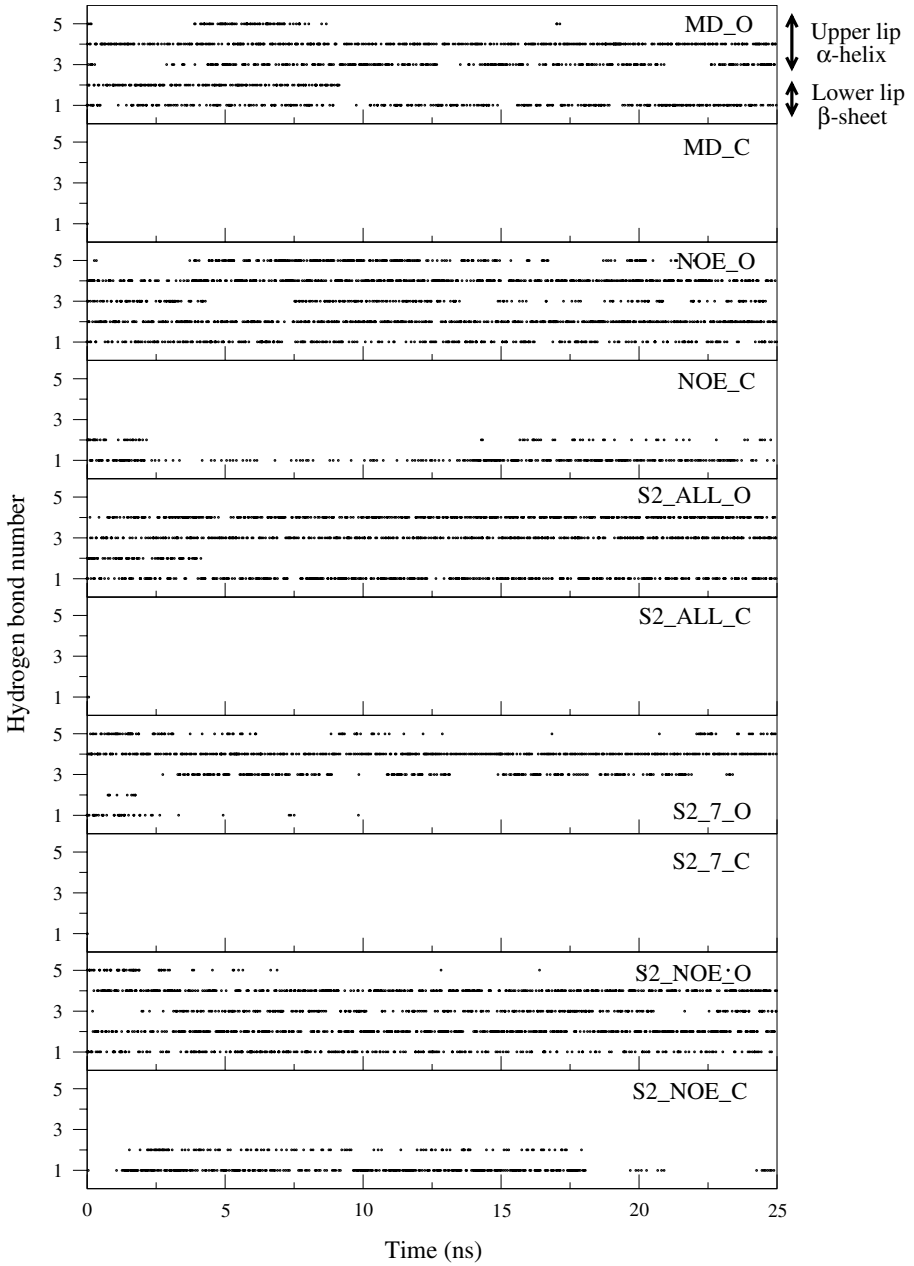

Fig. 3 Secondary structure hydrogen bonds present in the lower and upper lip regions during the simulations, from *top to bottom* MD_O, MD_C, NOE_O, NOE_C, S2_ALL_O, S2_ALL_C, S2_7_O, S2_7_C, S2_NOE_O and S2_NOE_C. The data shown are for the hydrogen bonds 53 NH–61 CO (1), 61 NH–53 CO (2) (lower lip β-sheet), 138 NH–134 CO (3), 139 NH-135 CO (4) and 140 NH–136 CO (5) (upper lip α-helix). A *circle* indicates that the hydrogen bond is present

all five secondary structure hydrogen bonds in the lip regions are present, although the helical hydrogen bonds 138NH-134CO (no. 3) and 140NH-136CO (no. 5) are both fluctuating with populations of 49 and 44 %, respectively (Fig. 3, 3rd panel). However, in the NOE_C simulation, although the two lower lip β-sheet hydrogen bonds (no. 1 and 2) are formed (populations 15–49 %), the helical hydrogen bonds are still missing in the upper lip region (Fig. 3, 4th panel). The NOE_O simulation shows significant fluctuations in the 58–131 (Fig. 6) and 19–131 (Fig. 5) Cα-Cα distances (2nd panel). At the start and end of this simulation, these distances are similar to those seen in the X-ray structure open conformation. However, between 10 and 20 ns, these distances decrease and are similar to those seen in the closed conformation. In contrast, in the NOE_C simulation, the fluctuations in these distances are much smaller. Their values never increase to those seen in the X-ray structure open conformation.

The lower and upper lip regions are known to be flexible in solution (Smith et al. 2013). Figure 7a, b compares the root-mean-square positional fluctuations of the backbone N atoms in the various simulations. Elevated RMSF values are seen in both the upper and lower lip regions in the MD_O (black, dotted), and NOE_O (red, dotted) simulations (maximum values of 0.29 and 0.37 nm in the lower and upper lip regions, respectively in the MD_O

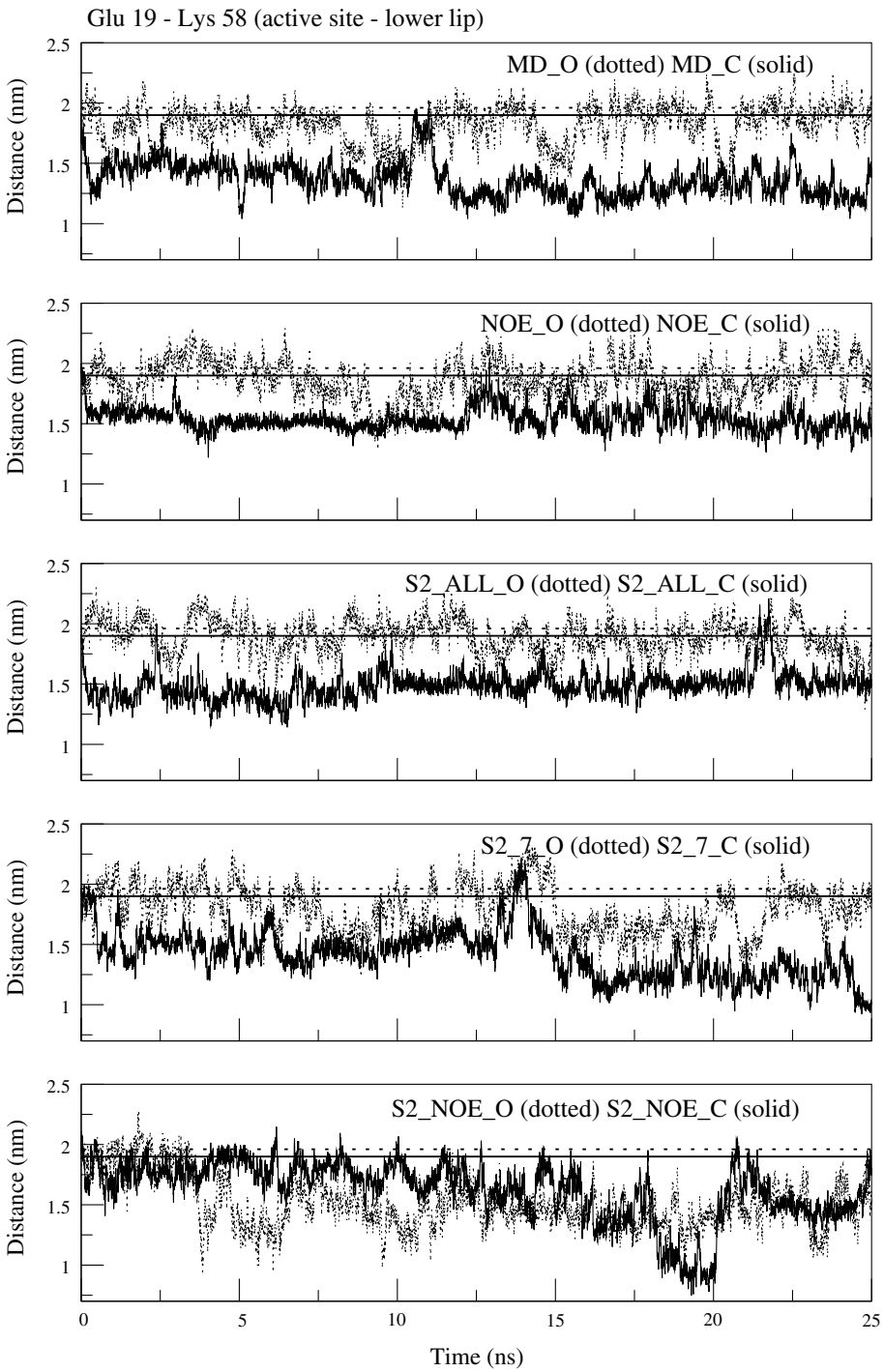

Fig. 4 Time series showing the variations in the distance between the Cα atoms of Glu 19 and Lys 58 through the simulations. From *top to bottom* the data for the unrestrained simulations (MD_O *dotted line*; MD_C *solid line*), the data for the simulations with NOE restraining (NOE_O *dotted line*; NOE_C *solid line*), the data for the simulations with order parameter restraining for all residues (S2_ALL_O *dotted line*; S2_ALL_C *solid line*), the data for the simulations with order parameter restraining for 7 residues (S2_7_O *dotted line*; S2_7_C *solid line*) and the data for the simulations with order parameter and NOE restraining (S2_NOE_O *dotted line*; S2_NOE_C *solid line*). In each panel, the distance in the X-ray structures with the open and closed conformation are shown by *thick dotted* and *solid horizontal lines*, respectively

simulation, and 0.31 and 0.38 nm in the lower and upper lip regions, respectively in the NOE_O simulation). However, a significantly smaller RMSF is seen in the upper lip region in the MD_C (black, solid) and NOE_C (red, solid) simulations (maximum values 0.16 nm). The RMSF in the lower lip is slightly larger in the MD_C simulation (maximum value 0.21 nm) and significantly larger in the NOE_C simulation (maximum value 0.29 nm) than in the upper lip.

Figure 7c, d compares the ^{1}H-^{15}N order parameters calculated from the MD_O (black, dotted), MD_C (black, solid), NOE_O (red, dotted) and NOE_C (red, solid) simulations with the experimental data (Smith et al. 2013). Overall, the experimental order parameters and those calculated from the MD_O and NOE_O simulations show a similar trend with low order parameter values seen at the termini, in the lower and upper lip regions and an exposed

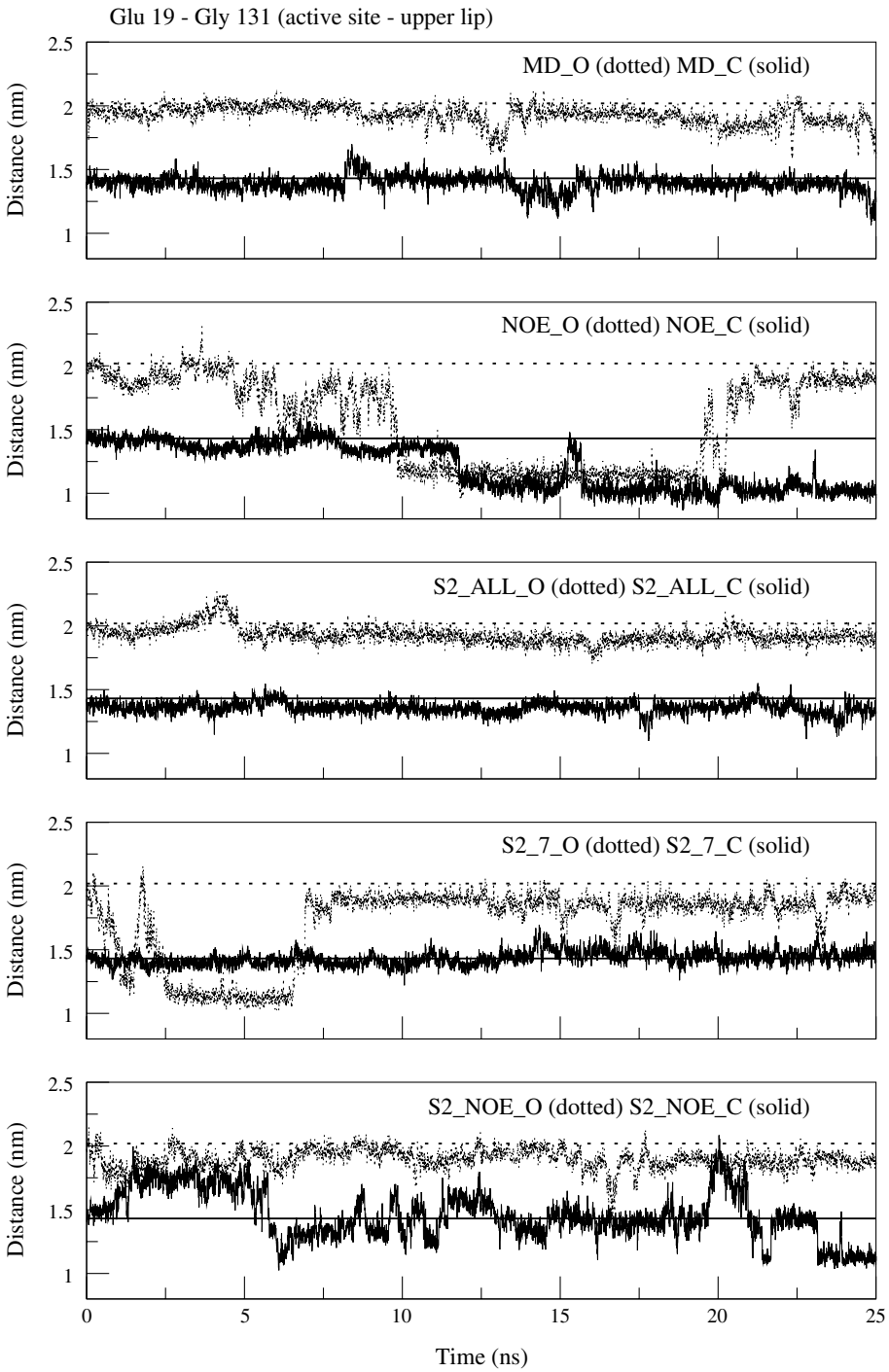

Fig. 5 Time series showing the variations in the distance between the Cα atoms of Glu 19 and Gly 131 through the simulations. From *top to bottom* the data for the unrestrained simulations (MD_O *dotted line*; MD_C *solid line*), the data for the simulations with NOE restraining (NOE_O *dotted line*; NOE_C *solid line*), the data for the simulations with order parameter restraining for all residues (S2_ALL_O *dotted line*; S2_ALL_C *solid line*), the data for the simulations with order parameter restraining for seven residues (S2_7_O *dotted line*; S2_7_C *solid line*) and the data for the simulations with order parameter and NOE restraining (S2_NOE_O *dotted line*; S2_NOE_C *solid line*). In each panel, the distance in the X-ray structures with the open and closed conformation are shown by *thick dotted* and *solid horizontal lines*, respectively

loop (residues 25–27) which shows elevated RMSF values. The experimental data has 44 residues with very large order parameter values in the range 0.96–1.0. The values calculated from the simulations for these residues are slightly lower in the range 0.89–0.93. This difference for residues with very large experimental order parameter values has also been observed in other comparisons of experimental data and those calculated from simulation trajectories (Buck et al. 2006; Koller et al. 2008; Soares et al. 2004). For the MD_C and NOE_C simulations large order parameters are seen in the lower lip region (0.69–0.80) compared to those seen in the MD_O and NOE_O simulations (0.38–0.62).

The lip regions in the NOE_O simulation sample a range of conformations, with elevated N atom root-mean-square positional fluctuations and significant fluctuations in the 19–131 (Fig. 5) and 58–131 (Fig. 6) distances. However, conformational sampling is more limited in the NOE_C

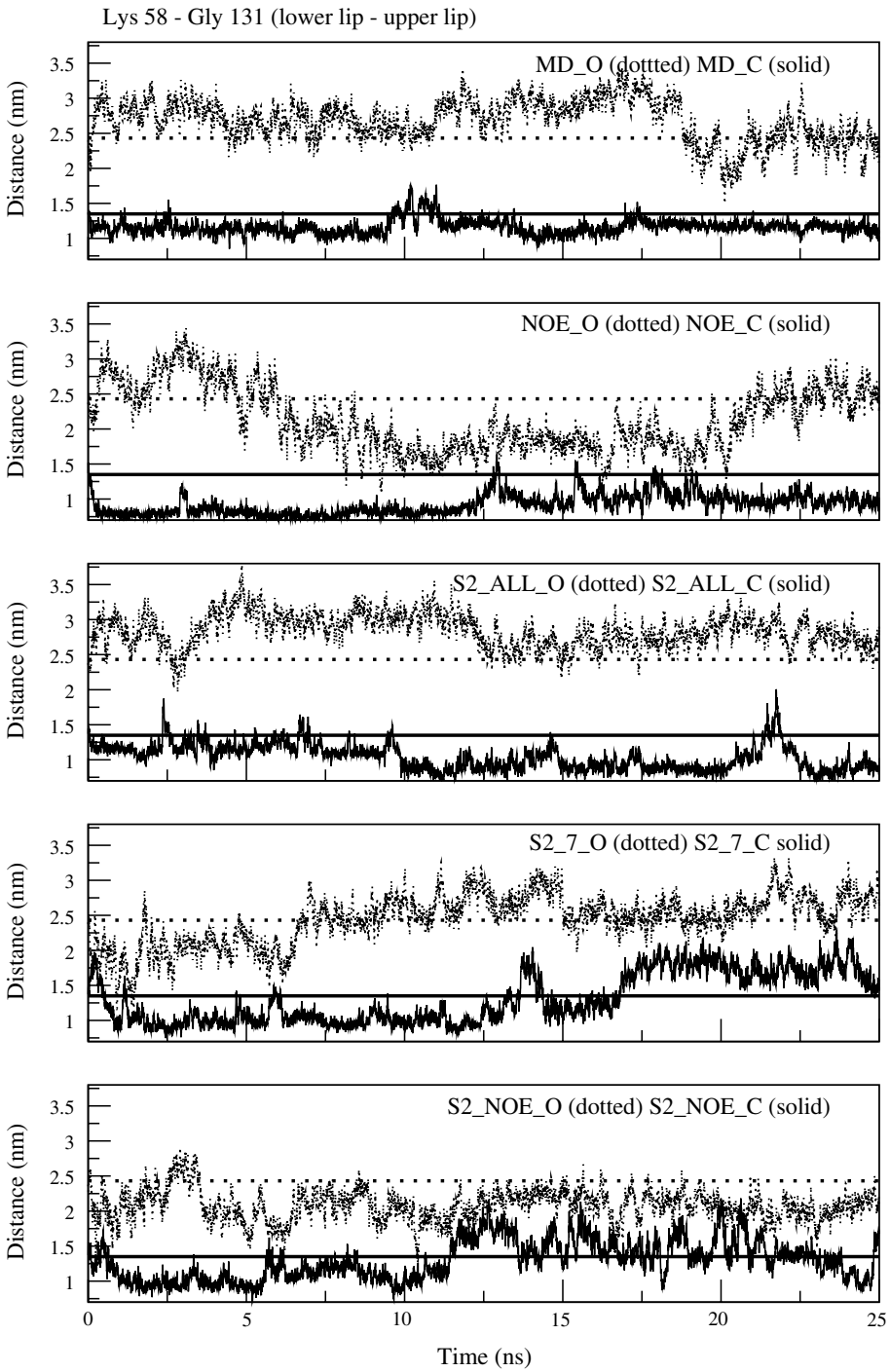

Fig. 6 Time series showing the variations in the distance between the Cα atoms of Lys 58 and Gly 131 through the simulations. From *top to bottom* the data for the unrestrained simulations (MD_O *dotted line*; MD_C *solid line*), the data for the simulations with NOE restraining (NOE_O *dotted line*; NOE_C *solid line*), the data for the simulations with order parameter restraining for all residues (S2_ALL_O *dotted line*; S2_ALL_C *solid line*), the data for the simulations with order parameter restraining for seven residues (S2_7_O *dotted line*; S2_7_C *solid line*) and the data for the simulations with order parameter and NOE restraining (S2_NOE_O *dotted line*; S2_NOE_C *solid line*). In each panel, the distance in the X-ray structures with the open and closed conformation are shown by *thick dotted* and *solid horizontal lines,* respectively

simulation, especially in the upper lip region where small N atom root-mean-square positional fluctuations are observed. In order to enhance the conformational sampling and to obtain convergence between properties calculated from simulations run from different starting structures, MD simulations were run with order parameter restraining (Hansen et al. 2014). Four simulations were run, two starting from the open conformation and two from the closed conformations in the X-ray structure, with time averaged ^{1}H-^{15}N order parameter restraints being applied. In the first pair of simulations (S2_ALL_O and S2_ALL_C; Table 1) the order parameters were restrained to the experimental values for all residues where experimental data are available (although a target value of 0.90 was used for residues with an experimental order parameter above this value, Table S2). In the second pair of simulations (S2_7_O and S2_7_C; Table 1) order parameter restraints were applied for the seven residues (28, 58, 59, 60, 135, 136, and 137, Table S3) which

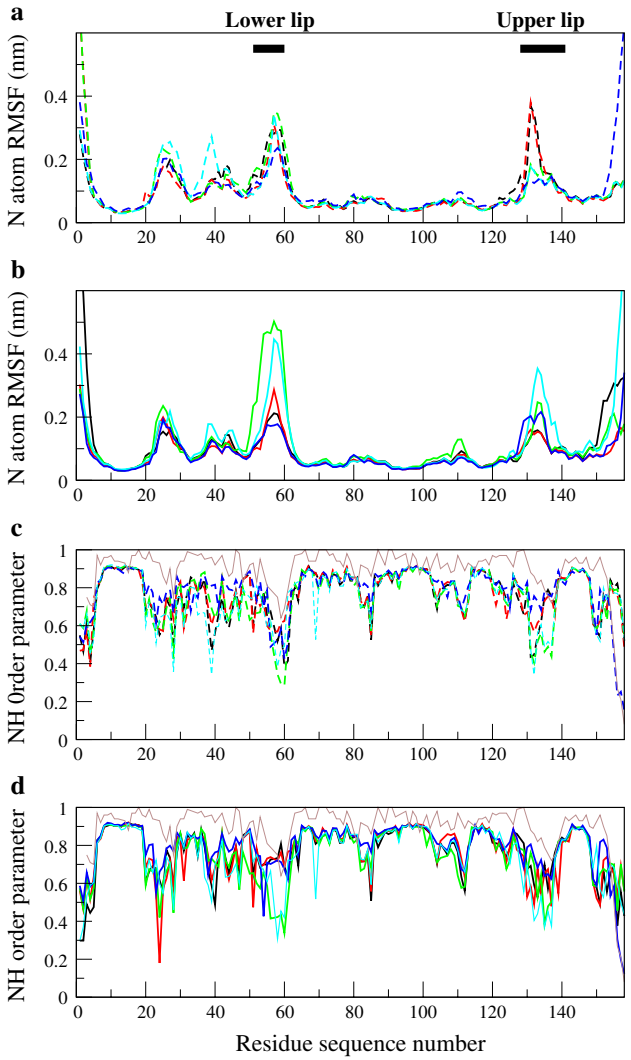

Fig. 7 The root-mean-square positional fluctuations (RMSF) of the backbone nitrogen atoms (A and B) and the ^{1}H-^{15}N order parameters (C and D) calculated from the unrestrained simulations (MD_O and MD_C, black) and simulations with NOE restraining (NOE_O and NOE_C, *red*), order parameter restraining for all residues (S2_ALL_O and S2_ALL_C, *blue*), order parameter restraining for seven residues (S2_7_O and S2_7_C, *green*) and order parameter and NOE restraining (S2_NOE_O and S2_NOE_C, *cyan*). The data for the simulations started from the open conformations are shown with *dotted* (O) *lines* in panels A and C while the data for the simulations started from the closed conformations are shown with *solid* (C) *lines* in panels B and D. The positions of the lower and upper lip regions in the sequence are indicated by *black bars* in panel A and the experimental order parameter values are shown in *brown* (*thin solid lines*) in panels C and D. In the calculations the time period 10–25 ns was used with, for the order parameter calculations, a 1 ns window. The structures were superimposed using the backbone of the residues in the core of α helices 1, 2, 3, and 5 (residues 8–17, 73–79, 90–99, and 115–118)

show, apart from the N and C-terminal residues, the lowest experimental ^{1}H-^{15}N order parameters (Smith et al. 2013), the target value being 0.45, the mean value seen for the lower lip residues in the MD_O simulation.

The ^{1}H-^{15}N order parameters calculated from the S2_ALL_O and S2_ALL_C simulations (blue, Fig. 7c, d) show trends similar to the experimental ones through the sequence although for residues with the largest experimental order parameters the calculated values are lower reflecting the target order parameter value of 0.90 for these residues. The lowest order parameter values seen in the lower and upper lip region are 0.43 and 0.68, respectively in the S2_ALL_O simulation and 0.43 and 0.62, respectively in the S2_ALL_C simulation. Overall, the data for the S2_ALL_O and S2_ALL_C simulations are similar to those for the corresponding unrestrained simulations MD_O and MD_C (black lines), although they show larger NOE bound violations (Fig. 2). In particular, both the S2_ALL_O and S2_ALL_C simulations show three NOE bound violations greater than 0.2 nm for the lower lip region. In addition, the RMSF values in the lower and upper lip regions in the S2_ALL_O simulation (maximum values of 0.24 and 0.14 nm, respectively) are smaller than those seen in the MD_O simulation (maximum values of 0.29 and 0.37 nm, respectively).

Both the S2_7_O and S2_7_C simulations show low ^{1}H-^{15}N order parameter values (0.28–0.50) for the seven residues where order parameter restraints have been applied (green, Fig. 7c, d). In addition, the S2_7_C simulation shows elevated N atom root-mean-square positional fluctuations in both the lower and upper loop regions (maximum values of 0.50 and 0.25 nm, respectively) while in the S2_7_O simulation only the values in the lower lip region are significantly elevated (maximum values of 0.35 nm and 0.17 nm in the lower and upper lip regions, respectively) (Fig. 7a, b). The larger fluctuations have, however, disrupted the secondary structure in the lip regions and large NOE violations are observed. In the S2_7_O simulation the populations of the β-sheet hydrogen bonds in the lower lip region have fallen to 3–7 % (no. 1, 2 in Fig. 3). In addition, in the upper lip region the populations of the helical hydrogen bonds 138NH- 134CO and 140NH- 136CO have been reduced to 42 and 20 %, respectively, while the 139NH-135CO hydrogen bond is still very persistent (91 % population; Fig. 3). In the S2_7_C simulation none of the secondary structure hydrogen bonds in the lip regions have a population greater than 0.1 % (Fig. 3). In addition, there are four and three NOE violations greater than 0.25 nm in the S2_7_O and S2_7_C simulations, respectively (Fig. 2).

In light of the large NOE violations observed in the S2_7_O and S2_7_C simulations, two further structure refinement simulations were run. These started from the open and closed conformations in the X-ray structure applying both the 22 NOE distance restraints for the lower and upper lip regions and the seven ^{1}H-^{15}N order parameter restraints (simulations S2_NOE_O and S2_NOE_C; Table 1). The ^{1}H-^{15}N order parameter values and N atom

root-mean-square positional fluctuations calculated from the S2_NOE_O and S2_NOE_C simulations are similar to those seen in the S2_7_O and S2_7_C simulations, respectively (Fig. 7). However, in both the S2_NOE_O and S2_NOE_C simulations, because NOE restraints have been applied in the structure refinement protocol, there are no NOE violations greater than 0.06 nm (Fig. 2). In addition, the two hydrogen bonds between β-strands in the lower lip region have a significant population (63–92 and 21–61 % in simulations S2_NOE_O and S2_NOE_C, respectively) (Fig. 3).

Discussion

The upper and lower lip regions show quite different behavior in the structure refinement MD simulations of λ-lysozyme reported here. The lower lip in general shows larger atom-positional RMSF values for the backbone N atoms than the upper lip. However, for the simulations starting from the closed conformation in the X-ray structure, order parameter restraining is needed to see this wider level of dynamics. The NOE distance bounds for the lower lip region are satisfied in the simulations only when NOE restraining is applied. Indeed, NOE restraining is essential for forming the β-strands in the lower lip in the simulation starting from the closed conformation and for maintaining the β-strands in the simulations starting from the open conformation with order parameter restraining. When both the order parameter and NOE restraints are applied in the simulations, the extent of sampling and range of conformers populated in the simulations starting from the open and closed conformations is more similar. For example, the fluctuations in the 19 Cα -58 Cα distance in the S2_NOE_O and S2_NOE_C simulations (Fig. 4) are comparable with mean values of 1.52 and 1.62 nm, respectively. It is interesting that highly persistent β-strand hydrogen bonds are seen in this lip region even though it is undergoing considerable dynamics.

In the upper lip region, the simulations starting from the open and closed conformations in the X-ray structure do not show complete convergence of properties. The α-helical hydrogen bonds at the end of this lip region and the start of helix α6 are seen in all the simulations starting from the open conformation. The helical secondary structure in this region is very fluctuating though, with the 140NH-136CO and 138NH-134CO hydrogen bonds having populations of 12–44 and 42–58 %, respectively. These α-helical hydrogen bonds are never seen in the simulations starting from the closed conformation. The differences between the conformations populated in the simulations starting from the open and closed conformations is also shown clearly in the 19-131 and 58-131 Cα-Cα distances analyzed (Figs. 5 and 6). Longer distances, seen in the simulations from the open conformation, are not observed in the S2_ALL_C, S2_7_C and S2_NOE_C simulations. Despite the conformational differences, all the simulations satisfy the NOE distance bounds in the upper lip region. In addition, in the S2_ALL_C, S2_7_C and S2_NOE_C simulations the fluctuations in the upper lip region have been significantly increased so the simulations also satisfy the order parameter data. Therefore, it is not clear from the experimental data and the simulations whether or not the upper lip region forms a significant population of α-helix in solution and if insufficient sampling is still preventing its formation in the simulations starting from the closed conformation.

Interestingly, an analysis of crystal contacts and intermolecular hydrogen bonds in the 1AM7 crystal structure of λ-lysozyme shows hydrogen bonds between Pro 57 and Lys 58 in the lower lip region of molecule B in the closed conformation and Asn 6 in molecule C. In addition, residues 131–134 in the upper lip region of both molecules A (open conformation) and B (closed conformation) also make hydrogen bonds to molecule C. These contacts may help stabilize the open and closed conformations seen in the crystal structure and explain, at least in part, the challenge of observing convergence between the MD simulations starting from the open and closed conformations reported here. Another explanation may lie in the limited length, 25 ns, of the simulations. As mentioned in the Introduction, exchange contributions to T_2 relaxation are also observed for certain residues in the lip regions, reflecting slower timescale motions (Smith et al. 2013). While open and closed conformation must have comparable (free) energies, they may be separated by an energy barrier that requires times in the microsecond time scale to be surpassed.

Overall, the simulations performed here have shown the value of restraining to experimental data in so-called structure refinement simulations. Unrestrained simulations starting from the open and closed conformations observed in a crystalline environment did not give the same values of the various properties analyzed and did not satisfy the NOE and order parameter data derived from experiments on the protein in solution. This stresses the importance of comparisons between MD simulation results and experimental data. A very conservative structure refinement approach has been used here, with only 22 NOE and either seven or 128 order parameter restraints being used with time averaging. The order parameter restraining has been essential for enhancing the positional fluctuations in the upper and lower lip regions, especially in the simulations starting from the closed conformation. Moreover, the combination of NOE and order parameter restraining worked well together, producing trajectories which agree with the experimental data and thus can be considered as a viable

structural representation of these. The simulations with order parameter and NOE restraining show a wide range of conformations in the lower and upper lip regions with maximum backbone N atom RMSF values of 0.34 and 0.18 nm in the upper and lower lip regions, respectively, in the S2_NOE_O simulation and of 0.46 and 0.35 nm in the upper and lower lip regions, respectively in the S2_NOE_C simulation (Fig. 7). The simulations therefore provide a fuller description of the structural properties of the protein in solution than can be obtained from the open and closed forms present in the X-ray crystal structures or from standard single-structure, i.e., non time-averaging, refinement based on NMR data.

Acknowledgments WFvG thanks the Swiss National Science Foundation, grant number 200020-137827 and its National Competence Center for Research (NCCR) in Structural Biology, and the European Research Council, grant number 228076, for financial support. NH thanks the German Research Foundation (DFG) for financial support within the Cluster of Excellence in Simulation Technology (EXC 310/1) at the University of Stuttgart. LJS acknowledges the use of the Advanced Research Computing resources at the University of Oxford in carrying out some of this work. We thank Christina Redfield and André Matagne for their help and advice regarding the experimental data for λ-lysozyme.

References

Bahar I, Lezon TR, Yang LW, Eyal E (2010) Global dynamics of proteins: Bridging between structure and function. In: Rees DC, Dill KA, Williamson JR (eds) Ann Rev Biophys, vol 39. pp 23-42. doi:10.1146/annurev.biophys.093008.131258

Berendsen HJC, Postma JPM, van Gunsteren WF, Hermans J (1981) Interaction models for water in relation to protein hydration. In: Pullman B (ed) Intermolecular forces. Reidel, Dordrecht, pp 331–342

Berendsen HJC, Postma JPM, van Gunsteren WF, Dinola A, Haak JR (1984) Molecular dynamics with coupling to an external bath. J Chem Phys 81:3684–3690. doi:10.1063/1.448118

Bienkowskaszewczyk K, Lipinska B, Taylor A (1981) The R-gene product of bacteriophage lambda is the murein transglycosylase. Mol Gen Genet 184:111–114. doi:10.1007/bf00271205

Black LW, Hogness DS (1969) The ENZ lysozyme of bacteriophage III ordering the cyanogen bromide peptides phage lambda. J Biol Chem 244:1982–1987

Boehr DD, Nussinov R, Wright PE (2009) The role of dynamic conformational ensembles in biomolecular recognition. Nat Chem Biol 5:789–796. doi:10.1038/nchembio.232

Buck M, Bouguet-Bonnet S, Pastor RW, MacKerell AD (2006) Importance of the CMAP correction to the CHARMM22 protein force field: dynamics of hen lysozyme. Biophys J 90:L36–L38. doi:10.1529/biophysj.105.078154

Di Paolo A, Duval V, Matagne A, Redfield C (2010) Backbone H-1, C-13, and N-15 resonance assignments for lysozyme from bacteriophage lambda. Biomol NMR Assign 4:111–114. doi:10.1007/s12104-010-9219-8

Eichenberger AP et al (2011) GROMOS++ software for the analysis of biomolecular simulation trajectories. J Chem Theory Comput 7:3379–3390. doi:10.1021/ct2003622

Evrard C, Declercq JP, Fastrez J (1997) Crystallization and preliminary X-ray analysis of bacteriophage lambda lysozyme in which all tryptophans have been replaced by aza-tryptophans. Acta Crystallogr Sect D-Biol Crystallogr 53:217–219. doi:10.1107/s0907444996011523

Evrard C, Fastrez J, Declercq JP (1998) Crystal structure of the lysozyme from bacteriophage lambda and its relationship with V and C-type lysozymes. J Mol Biol 276:151–164. doi:10.1006/jmbi.1997.1499

Evrard C, Fastrez J, Soumillion P (1999) Histidine modification and mutagenesis point to the involvement of a large conformational change in the mechanism of action of phage lambda lysozyme. FEBS Lett 460:442–446. doi:10.1016/s0014-5793(99)01395-2

Frauenfelder H, Sligar SG, Wolynes PG (1991) The energy landscapes of motions of proteins. Science 254:1598–1603. doi:10.1126/science.1749933

Fuxreiter M (2012) Fuzziness: linking regulation to protein dynamics. Mol BioSyst 8:168–177. doi:10.1039/c1mb05234a

Hansen N, Heller F, Schmid N, van Gunsteren WF (2014) Time-averaged order parameter restraints in molecular dynamics simulations. J Biomol NMR 60:169–187. doi:10.1007/s10858-014-9866-7

Heinz TN, van Gunsteren WF, Hunenberger PH (2001) Comparison of four methods to compute the dielectric permittivity of liquids from molecular dynamics simulations. J Chem Phys 115:1125–1136. doi:10.1063/1.1379764

Henzler-Wildman K, Kern D (2007) Dynamic personalities of proteins. Nature 450:964–972. doi:10.1038/nature06522

Henzler-Wildman KA, Lei M, Thai V, Kerns SJ, Karplus M, Kern D (2007) A hierarchy of timescales in protein dynamics is linked to enzyme catalysis. Nature 450:913–916. doi:10.1038/nature06407

Jespers L, Sonveaux E, Fastrez J (1992) Is the bacteriophage-lambda lysozyme an evolutionary link or a hybrid between the C-type and V-type lysozymes-homology analysis and detection of the catalytic amino acid residues. J Mol Biol 228:529–538. doi:10.1016/0022-2836(92)90840-g

Kabsch W, Sander C (1983) Dictionary of protein secondary structure–pattern recognition of hydrogen bonded and geometrical features. Biopolymers 22:2577–2637. doi:10.1002/bip.360221211

Koller AN, Schwalbe H, Gohlke H (2008) Starting structure dependence of NMR order parameters derived from MD simulations: implications for judging force-field quality. Biophys J 95:L4–L6. doi:10.1529/biophysj.108.132811

Krissinel E, Henrick K (2007) Inference of macromolecular assemblies from crystalline state. J Mol Biol 372:774–797. doi:10.1016/j.jmb.2007.05.022

Leung AKW, Duewel HS, Honek JF, Berghuis AM (2001) Crystal structure of the lytic transglycosylase from bacteriophage lambda in complex with hexa-*N*-acetylchitohexaose. Biochemistry 40:5665–5673. doi:10.1021/bi0028035

Lewney S, Smith LJ (2012) Characterization of an alternative low energy fold for bovine α-lactalbumin formed by disulfide bond shuffling. Protein Struct Funct Bioinform 80:913–919. doi:10.1002/prot.23247

Motlagh HN, Wrabl JO, Li J, Hilser VJ (2014) The ensemble nature of allostery. Nature 508:331–339. doi:10.1038/nature13001

Ryckaert JP, Ciccotti G, Berendsen HJC (1977) Numerical integration of Cartesian equations of motion of a system with constraints-molecular dynamics of *n*-alkanes. J Comput Phys 23:327–341. doi:10.1016/0021-9991(77)90098-5

Schmid N, Allison JR, Dolenc J, Eichenberger AP, Kunz A-PE, van Gunsteren WF (2011a) Biomolecular structure refinement using the GROMOS simulation software. J Biomol NMR 51:265–281. doi:10.1007/s10858-011-9534-0

Schmid N, Eichenberger AP, Choutko A, Riniker S, Winger M, Mark AE, van Gunsteren WF (2011b) Definition and testing of the

GROMOS force-field versions 54A7 and 54B7. Eur Biophys J with Biophys Lett 40:843–856. doi:10.1007/s00249-011-0700-9

Schmid N, Christ CD, Christen M, Eichenberger AP, van Gunsteren WF (2012) Architecture, implementation and parallelisation of the GROMOS software for biomolecular simulation. Comput Phys Commun 183:890–903. doi:10.1016/j.cpc.2011.12.014

Sekhar A, Kay LE (2013) NMR paves the way for atomic level descriptions of sparsely populated, transiently formed biomolecular conformers. Proc Natl Acad Sci USA 110:12867–12874. doi:10.1073/pnas.1305688110

Smith LJ, Bowen AM, Di Paolo A, Matagne A, Redfield C (2013) The dynamics of Lysozyme from bacteriophage lambda in solution probed by NMR and MD simulations. ChemBioChem 14:1780–1788. doi:10.1002/cbic.201300193

Smock RG, Gierasch LM (2009) Sending signals dynamically. Science 324:198–203. doi:10.1126/science.1169377

Soares TA, Daura X, Oostenbrink C, Smith LJ, van Gunsteren WF (2004) Validation of the GROMOS force-field parameter set 45A3 against nuclear magnetic resonance data of hen egg lysozyme. J Biomol NMR 30:407–422. doi:10.1007/s10858-004-5430-1

Soumillion P, Fastrez J (1998) Incorporation of 1,2,4-triazole-3-alanine into a mutant of phage lambda lysozyme containing a single histidine. Protein Eng 11:213–217. doi:10.1093/protein/11.3.213

Taylor A, Das BC, Vanheijenoort J (1975) Bacterial cell-wall peptidoglycan fragments produced by phage lambda or VI II endolysin and containing 1,6-anhydro-*N*-acetylmuramic acid. Eur J Biochem 53:47–54. doi:10.1111/j.1432-1033.1975.tb04040.x

Tironi IG, Sperb R, Smith PE, van Gunsteren WF (1995) A generalised reaction field method for molecular dynamics simulations. J Chem Phys 102:5451–5459. doi:10.1063/1.469273

Tokuriki N, Tawfik DS (2009) Protein dynamism and evolvability. Science 324:203–207. doi:10.1126/science.1169375

van Gunsteren WF et al (1996) Biomolecular simulation: the GROMOS96 manual and user guide. Vdf Hochschulverlag AG an der ETH Zürich, Switzerland